Activation cross sections of deuteron-induced reactions on praseodymium up to 24 MeV

Masayuki Aikawa [a,*], Takuto Maehashi [b], Dagvadorj Ichinkhorloo [a], Shuichiro Ebata [c], Yukiko Komori [d], Hiromitsu Haba [d]

[a] *Faculty of Science, Hokkaido University, Sapporo 060-0810, Japan*

[b] *School of Science, Hokkaido University, Sapporo 060-0810, Japan*

[c] *Graduate School of Science and Engineering, Saitama University, Saitama 338-8570, Japan*

[d] *Nishina Center for Accelerator-Based Science, RIKEN, Wako 351-0198, Japan*

Abstract

We measured activation cross sections of deuteron-induced reactions on ^{141}Pr. The production cross sections of ^{141,140}Nd, ^{142}Pr, and ^{139}Ce were determined up to 24 MeV using the stacked-foil activation technique and high-resolution γ-ray spectrometry. The derived cross sections were compared with experimental data studied earlier and theoretical model calculations. Our results are consistent with part of the previous data.

Keyword

Neodymium-140; Praseodymium-140; Praseodymium-142; Praseodymium target; Deuteron irradiation; Cross section; Excitation function

1. Introduction

Radionuclides are used for diagnostic and therapeutic nuclear medicine. Investigation on the production of such medical radionuclides is indispensable for development of the application. The radionuclides ^{140}Nd ($T_{1/2}$ = 3.37 d) and ^{142}Pr ($T_{1/2}$ = 19.12 h) are expected as a ^{140}Nd/^{140}Pr generator for Positron Emission Tomography (PET) [1] and treatment for arteriovenous malformations [2], respectively. These radionuclides can simultaneously be formed using some charged-particle-induced reactions. We focused on the deuteron-induced reaction on the monoisotopic element ^{141}Pr. In a literature survey, four experimental studies of the reaction were found [3–6]. The experimental cross sections published in the literature are somewhat scattered. Therefore, we conducted experiments to measure the cross sections of the reaction. The production cross sections of ^{141,140}Nd, ^{142}Pr, and ^{139}Ce were determined up to 24 MeV. The results are expected to contribute to development of the nuclear medicine.

* Corresponding author: Masayuki AIKAWA (aikawa@sci.hokudai.ac.jp), Faculty of Science, Hokkaido University, Sapporo 060-0810, Japan

2. Experimental

Two independent experiments to measure activation cross sections of the deuteron-induced reaction on ^{141}Pr were conducted. The 24 MeV deuteron beams were extracted from the K70-MeV AVF cyclotron at RIKEN. The stacked-foil activation technique and high-resolution γ-ray spectrometry were adopted for the experiments.

Two targets were composed of pure metallic foils of ^{141}Pr, ^{nat}Ti and ^{27}Al. The first and second target stacks were composed of pure metallic foils of ^{141}Pr and ^{nat}Ti (#1) and ^{141}Pr, ^{nat}Ti and ^{27}Al (#2), respectively. The ^{nat}Ti foils were interleaved for the $^{nat}Ti(d,x)^{48}V$ monitor reaction to assess the beam parameters and the target thicknesses. The ^{27}Al foils were used for energy degradation variation and catching recoiled products.

Two ^{141}Pr (purity: 99%, thickness: 100 μm, size: 25 × 25 mm^2), two ^{nat}Ti (purity: 99.6%, thickness: 5 μm, size: 50 × 100 mm^2) and one ^{27}Al (purity: >99%, thickness: 5 μm, size: 100 × 100 mm^2) foils were purchased from Nilaco Corp., Japan. The ^{141}Pr foils sealed under argon were unpacked one day before beam irradiation to minimize oxidation. The surface area and weight of each foil were measured. The thicknesses of the foils were determined as 67.6 and 72.3 mg/cm^2 for ^{141}Pr, 2.3 mg/cm^2 for ^{nat}Ti and 1.5 mg/cm^2 for ^{27}Al. The foils were cut into a small size of 8 × 8 mm^2 to fit target folders. Nine sequential sets of Pr-Ti-Ti or Pr-Al-Ti-Ti-Al foils (27 or 45 foils in total) were stacked into the target folders served as the Faraday cups.

The stacked targets were irradiated with deuteron beams collimated to a 3 mm diameter for 30 min. The average beam intensities of 107 and 110 nA for the stacks #1 and #2, respectively, were measured by the Faraday cups without electron suppressors. The beam loss and dispersion in the targets were neglected. The primary beam energies of 24.1 and 24.3 MeV were determined for the stacks #1 and #2, respectively, using the time-of-flight method [7]. Energy degradation of the beams in the stacked targets was calculated using stopping powers obtained from the SRIM code [8].

γ rays emitted from the irradiated foils without chemical separation were measured using a high-purity germanium detector (ORTEC GEM30P4-70) and analyzed by a dedicated software (SEIKO EG&G Gamma Studio). The efficiency of the detector was calibrated with a multiple γ-ray emitting point source (Eckert & Ziegler Isotope Products) consisting of the eight radionuclides, $^{57,60}Co$, ^{88}Y, ^{109}Cd, ^{113}Sn ^{137}Cs, ^{139}Ce and ^{241}Am. Each ^{141}Pr foil was measured together with the next foil to correct the recoil loss. The ^{141}Pr foils were measured seven and eight times after cooling times from 2.2 h to 40.2 d for the stack #1 and from 3.2 h to 40.6 d for #2. The dead time was kept below 5.2%. Required nuclear data were retrieved from the online databases, NuDat 2.8 [9], LiveChart [10], and QCalc [11]. The nuclear data were summarized in Table 1.

Cross sections of the $^{nat}Ti(d,x)^{48}V$ monitor reaction were derived to assess the beam parameters and the target thicknesses. The cross sections were determined using the measurement of the 983.5-keV γ line (I_γ = 99.98%). The results were compared with the IAEA recommended values [12,13]. According to the comparison, the thicknesses of the ^{141}Pr foils were all increased by 1% within the uncertainties (2%). The measured beam intensities and the thicknesses of ^{nat}Ti and ^{27}Al were adopted without any correction for deduction of the cross sections. The cross sections using the corrected experimental parameters agree with the recommended values as shown in Fig. 1. All the experimental parameters adopted to determine the cross sections were listed in Table 2.

Table 1. Reaction and decay data retrieved from online databases [9–11]

Nuclide	Half-life	Decay mode (%)	E_γ (keV)	I_γ (%)	Contributing reaction	Q-value (MeV)
^{141}Nd	2.49 h	$\varepsilon+\beta^+$ (100)	**1126.91**	0.80(3)	^{141}Pr(d,2n)	-4.8
^{140}Nd	3.37 d	ε (100)	-	-	^{141}Pr(d,3n)	-12.8
^{140}Pr	3.39 min	$\varepsilon+\beta^+$ (100)	**511.0**	102.0(6)	^{141}Pr(d,t)	-3.1
			1596.1	0.49(4)	^{140}Nd decay	
^{142}Pr	19.12 h	β^- (99.9836)	**1575.6**	3.7(4)	^{141}Pr(d,p)	3.6
		ε (0.0164)				
^{139}Ce	137.641 d	ε (100)	**165.8575**	80(8)	^{141}Pr(d,α)	11.6
					^{141}Pr(d,nt)^{139}Pr(ε)	-11.1
					^{141}Pr(d,4n)^{139}Nd(ε)^{139}Pr(ε)	-23.2
^{48}V	15.97 d	$\varepsilon+\beta^+$ (100)	511.0	99.8(8)	^{nat}Ti(d,x)	
			983.53	99.98(4)		
			1312.106	98.2(3)		

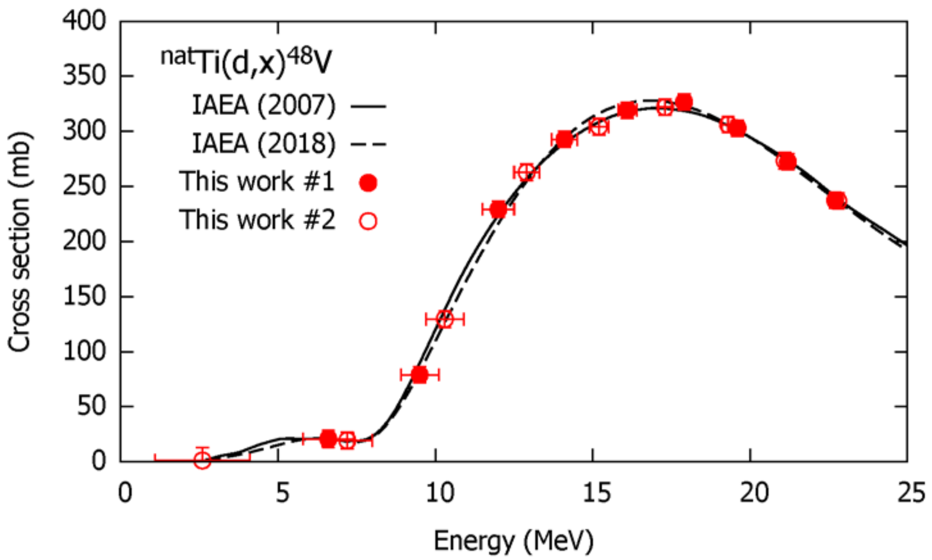

Fig. 1. Excitation function of the ^{nat}Ti(p,x)^{48}V monitor reaction compared with the recommended values [12,13]. Some error bars are smaller than the symbol size.

Table 2. Experimental parameters

Experiment No.	#1	#2
Target		
Measured (corrected) thickness (mg/cm^2)	Pr: 67.6 (68.2)	Pr: 72.3 (73.0)
	Ti: 2.3	Ti: 2.3
		Al: 1.5
Stack composition	9 sets of Pr-Ti-Ti foils	9 sets of Pr-Al-Ti-Ti-Al foils
Beam		
Current (nA)	107	110
Primary energy (MeV)	24.1 ±0.1	24.3 ±0.1
Irradiation time (min)	30	30
Measurement		
Series: Cooling time (Distance)	Ser. 1: 2.2-3.7 h (100 cm)	Ser. 1: 3.2-4.7 h (50 cm)
	Ser. 2: 3.9-6.4 h (50 cm)	Ser. 2: 4.9-12 h (5-50 cm)
	Ser. 3: 6.9-25 h (20-50 cm)	Ser. 3: 13-47 h (5-50 cm)
	Ser. 4: 1.4-2.3 d (10-50 cm)	Ser. 4: 1.4-3.4 d (5-50 cm)
	Ser. 5: 2.4-3.3 d (5-50 cm)	Ser. 5: 3.5 d (5-30 cm)
	Ser. 6: 3.7-4.9 d (5-20 cm)	Ser. 6: 3.8-3.9 d (30 cm)
	Ser. 7: 40 d (3 cm)	Ser. 7: 3.9-4.0 d (30 cm)
		Ser. 8: 40-41 d (3 cm)

3. Results and discussion

The production cross sections of ^{141,140}Nd, ^{142}Pr, and ^{139}Ce were determined for the deuteron-induced reaction on ^{141}Pr. The derived cross sections are summarized in Tables 3 and 4. The results are graphically shown in Figs. 2-5 with the previous experimental data [3,5,6] and the theoretical model calculation in the TENDL-2019 library [14].

The median projectile energy in each foil is listed in Tables 3 and 4 with the total uncertainty and the energy thickness in parentheses. The total energy uncertainties of 0.1-0.7 MeV and 0.1-1.1 MeV were propagated from the uncertainties of the primary beam energies (0.1 MeV) and the target thicknesses (1-2%). The estimated energy thicknesses of the ^{141}Pr foils were 0.7-1.3 MeV and 0.7-1.9 MeV for the stacks #1 and #2, respectively. The total uncertainties of the cross sections, 8.4-13.8% for the stack #1 and 7.4-15.5% for #2, are the square roots of the quadratic summation of the components; beam intensity (5%), γ-ray intensity (0.6-10.8%), detector efficiency (5-6%), target thickness (1-2%), target purity (1%) and counting statistics (0.2-7.2% and 0.5-11.1%).

Table 3. Production cross sections derived in the first experiment (#1)

Energy (MeV)	^{141}Nd (mb)	^{140}Nd (mb)	^{142}Pr (mb)	^{139}Ce (mb)
23.4 ±0.1 (±0.7)	401 ±34	915 ±107	91.2 ±12.2	4.98 ±0.62
22.0 ±0.1 (±0.7)	494 ±43	790 ±93	98.1 ±13.0	4.50 ±0.56
20.4 ±0.2 (±0.7)	658 ±56	583 ±70	109 ±14	4.27 ±0.53
18.8 ±0.2 (±0.8)	839 ±71	375 ±44	121 ±16	4.13 ±0.52
17.0 ±0.3 (±0.8)	1002 ±84	147 ±17	146 ±19	4.12 ±0.52
15.2 ±0.3 (±0.9)	1016 ±86	22.0 ±2.9	171 ±22	3.85 ±0.48
13.1 ±0.4 (±1.0)	834 ±70		201 ±26	3.10 ±0.39
10.8 ±0.5 (±1.1)	535 ±45		224 ±29	1.71 ±0.22
8.2 ±0.7 (±1.3)	126 ±11		127 ±17	0.330 ±0.041

Table 4. Production cross sections derived in the second experiment (#2)

Energy (MeV)	^{141}Nd (mb)	^{140}Nd (mb)	^{142}Pr (mb)	^{139}Ce (mb)
23.6 ±0.1 (±0.7)	385 ±34	852 ±69	88.2 ±12.0	5.29 ±0.67
21.9 ±0.1 (±0.7)	475 ±42	681 ±55	91.5 ±12.4	4.54 ±0.57
20.2 ±0.2 (±0.8)	740 ±65	581 ±47	119 ±16	4.79 ±0.60
18.3 ±0.2 (±0.8)	908 ±79	279 ±23	127 ±17	4.31 ±0.54
16.3 ±0.3 (±0.9)	1146 ±97	81.2 ±6.7	167 ±22	4.38 ±0.55
14.1 ±0.4 (±1.0)	924 ±77	3.73 ±0.34	174 ±23	3.63 ±0.46
11.7 ±0.5 (±1.1)	702 ±59	0.338 ±0.047	223 ±29	2.38 ±0.30
8.8 ±0.7 (±1.4)	234 ±20		173 ±23	0.622 ±0.084
5.1 ±1.1 (±1.9)	1.56 ±0.16		8.39 ±1.10	0.0291 ±0.0045

3.1 The ^{141}Pr(d,2n)^{141}Nd reaction

The cross sections of the ^{141}Pr(d,2n)^{141}Nd reaction were determined using the γ line at 1124.91 keV (I_γ = 0.80%) from the decay of ^{141}Nd ($T_{1/2}$ = 2.49 h). Almost all co-produced ^{141}Nd in the short-lived metastable state ($T_{1/2}$ = 62.0 s, IT: 100.00%, ε: <0.05%) decayed to the ground state during cooling times of 3.9-6.4 h and 4.9-11.9 h for the stacks #1 and #2, respectively. The results are compared with the previous study [5] and the TENDL-2019 values [14] as shown in Fig. 2. The previous experimental data are slightly larger than ours. The TENDL-2019 values show a similar shape to ours although the amplitude is slightly larger than ours.

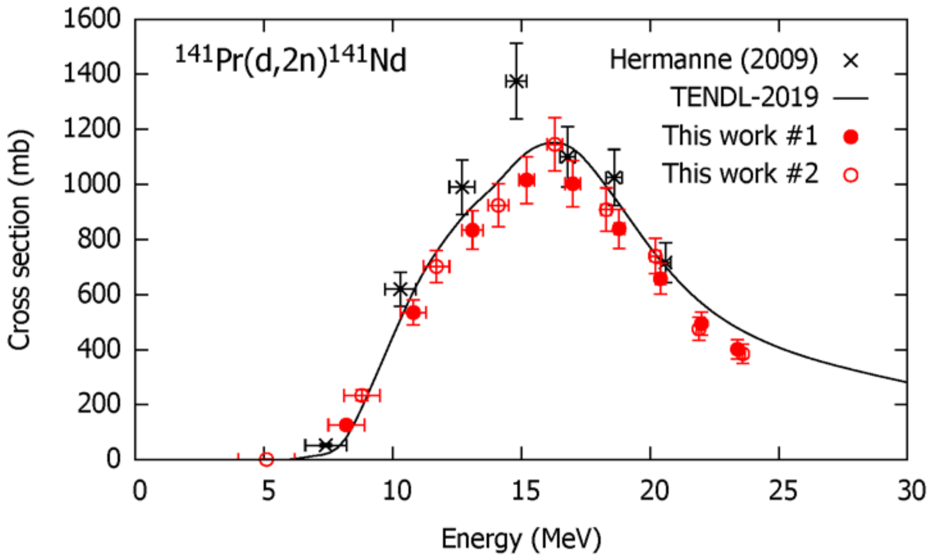

Fig. 2. Cross sections of the ^{141}Pr(d,2n)^{141}Nd reaction in comparison with the previous data [5] and the TENDL-2019 values [14].

3.2 The ^{141}Pr(d,3n)^{140}Nd reaction

There are no γ lines with the decay of ^{140}Nd ($T_{1/2}$ = 3.37 d). The γ line at 1596.1 keV (I_{γ} = 0.49%) from the decay of ^{140}Pr ($T_{1/2}$ = 3.39 min) was instead measured taking into account the secular equilibrium. The directly produced ^{140}Pr decayed soon after the end-of-bombardment. The γ rays of 1596.1 keV could also be emitted with the decay of energetically possible co-produced ^{140}La ($T_{1/2}$ = 1.67855 d, I_{γ} = 95.40%). However, we could confirm negligible contribution of ^{140}Nd to the 1596.1-keV γ peak based on the decay curve analyses (Ser. 2-6 for #1 and Ser. 2-4 for #2 in Table 2).

The cross sections of the ^{141}Pr(d,3n)^{140}Nd reaction in the first experiment were deduced from the γ line at 1596.1 keV because positrons with the ^{140}Pr decay could be emitted out from the foils and measured net counts of the 511.0-keV γ line were inconsistent with the actual activity. In the second experiment, we used copper plates to annihilate the emitted positrons. The two γ lines from the foils sandwiched between the copper plates were measured. The contributions of other positron emitters ^{141}Nd ($T_{1/2}$ = 2.49 h) and ^{139}Pr ($T_{1/2}$ = 4.41 h) to the annihilation γ line were negligible after a cooling time of 3.9-4.0 d. That of ^{22}Na formed in the Al catcher foils was also neglected due to small cross sections below 24 MeV (≦0.18 mb) [13] and its long half-life ($T_{1/2}$ = 2.6018 y). We confirmed the consistency of the cross sections derived using the two different γ lines.

The derived cross sections of the ^{141}Pr(d,3n)^{140}Nd reaction are shown in Fig. 3. The results are compared with the previous studies [5,6] and the TENDL-2019 values [14]. The data of Hermanne et al. (2009) agree with ours although the data of Lange (1968) are scattered and slightly larger than other experimental data below 24 MeV. The TENDL-2019 values are larger than ours.

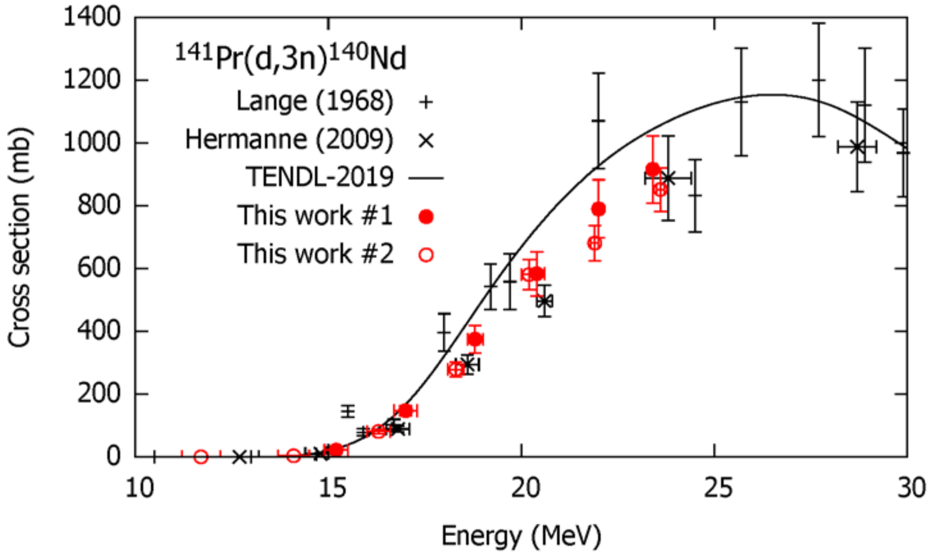

Fig. 3. Cross sections of the ^{141}Pr(d,3n)^{140}Nd reaction in comparison with the previous data [5,6] and the TENDL-2019 values [14].

3.3 The $^{141}Pr(d,p)^{142}Pr$ reaction

The excitation function of the $^{141}Pr(d,p)^{142}Pr$ reaction was derived from measurements of the γ line at 1575.6 keV (I_γ = 3.7%) from the decay of ^{142}Pr ($T_{1/2}$ = 19.12 h). The measurements were performed after cooling times of 6.9-25.1 h for stack #1 and 12.8-47.3 h for #2. During the cooling times, co-produced ^{142}Pr in the short-lived metastable state ($T_{1/2}$ = 14.6 min, IT: 100%) decayed completely to the ground state. The cumulative cross sections were shown in Fig. 3 with the experimental data studied earlier [3,5,6] and the TENDL-2019 values [14]. The experimental data in the three previous studies are slightly scattered, but almost consistent with ours within the uncertainties. The TENDL-2019 values are lower than all the experimental data including ours.

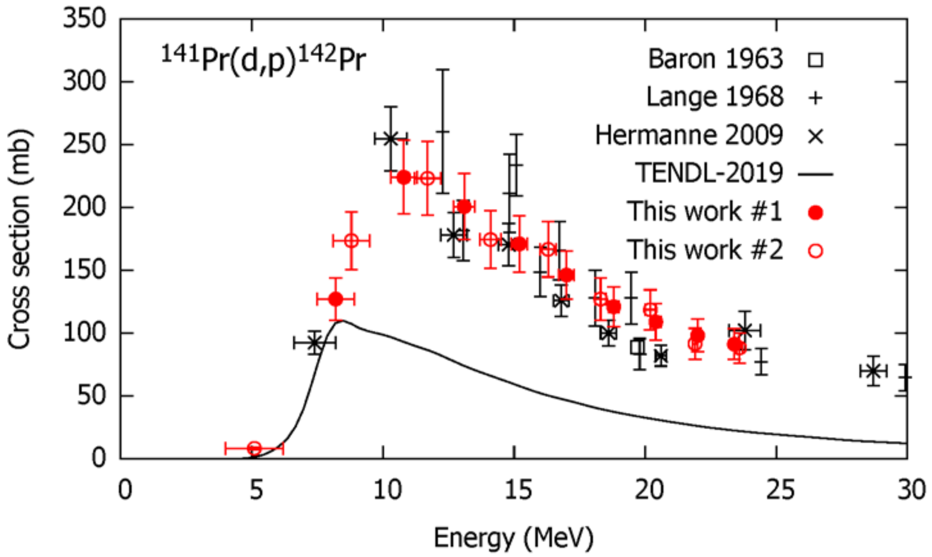

Fig. 4. Cross sections of the $^{141}Pr(d,p)^{142}Pr$ reaction in comparison with the previous data [3,5,6] and the TENDL-2019 values [14].

3.4 The ^{141}Pr(d,x)^{139}Ce reaction

The cumulative cross sections of the ^{141}Pr(d,x)^{139}Ce reaction were derived from the measurements of the 165.8575-keV γ line ($I_γ$ = 80%) emitted with the ^{139}Ce decay ($T_{1/2}$ = 137.641 d). There were possible contributions from co-produced ^{139}Ce in the metastable state ($T_{1/2}$ = 54.8 s), ^{139}Nd ($T_{1/2}$ = 29.7 min) and ^{139}Pr ($T_{1/2}$ = 4.41 h), which decayed during cooling times of 40 d. The results are shown in Fig. 5 in comparison with the previous data [5] and the TENDL-2019 values [14]. The previous data are in good agreement with ours. The TENDL-2019 values are larger than the experimental data.

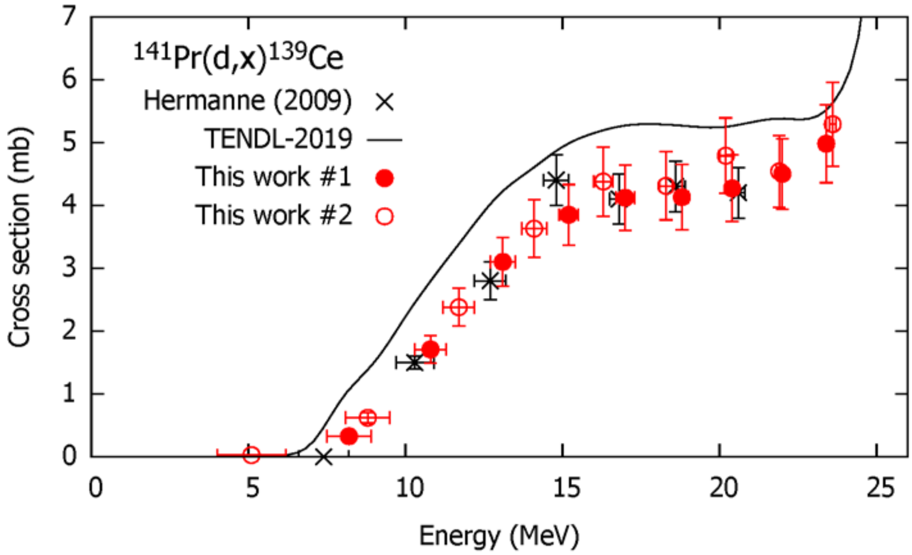

Fig. 5. Cross sections of the ^{141}Pr(d,x)^{139}Ce reaction in comparison with the previous data [5] and the TENDL-2019 values [14].

4. Summary

We measured activation cross sections of the deuteron-induced reaction on ^{141}Pr at the RIKEN AVF cyclotron. The production cross sections of ^{141,140}Nd, ^{142}Pr, and ^{139}Ce were determined using the well-established methods, stacked-foil activation technique and high-resolution γ-ray spectrometry. The derived cross sections are compared with the previous studies and the theoretical model calculation in the TENDL-2019 library. Our results are almost consistent with the previous study of Hermanne et al. (2009). The experimental results are valuable and expected to contribute to research and development of nuclear medicine.

Acknowledgement

This work was carried out at RI Beam Factory operated by RIKEN Nishina Center and CNS, University of Tokyo, Japan.

Declarations of interest

None

Reference

[1] K.P. Zhernosekov, D. V. Filosofov, S.M. Qaim, F. Rosch, A ^{140}Nd/^{140}Pr radionuclide generator based on physico-chemical transitions in ^{140}Pr complexes after electron capture decay of ^{140}Nd-DOTA, Radiochim. Acta. 95 (2007) 319–327. https://doi.org/10.1524/ract.2007.95.6.319.

[2] S.W. Lee, W.D. Reece, Dose calculation of ^{142}Pr microspheres as a potential treatment for arteriovenous malformations, Phys. Med. Biol. 50 (2005) 151–166. https://doi.org/10.1088/0031-9155/50/1/012.

[3] N. Baron, B.L. Cohen, Activation cross-section survey of deuteron-induced reactions, Phys. Rev. 129 (1963) 2636–2642. https://doi.org/10.1103/PhysRev.129.2636.

[4] A. Hermanne, F. Tárkányi, S. Takács, F. Ditrói, Extension of excitation functions up to 50 MeV for activation products in deuteron irradiations of Pr and Tm targets, Nucl. Instruments Methods Phys. Res. Sect. B. 383 (2016) 81–88. https://doi.org/10.1016/j.nimb.2016.06.010.

[5] A. Hermanne, F. Tárkányi, S. Takács, F. Ditrói, M. Baba, T. Ohtshuki, I. Spahn, A. V. Ignatyuk, Excitation functions for production of medically relevant radioisotopes in deuteron irradiations of Pr and Tm targets, Nucl. Instruments Methods Phys. Res. Sect. B. 267 (2009) 727–736. https://doi.org/10.1016/j.nimb.2008.12.017.

[6] V.J. Lange, H. Münzel, Bestimmung einiger Anregungsfunktionen für Deuteronenreaktionen mit ^{141}Pr, Radiochim. Acta. 9 (1968) 66–71. https://doi.org/doi.org/10.1524/ract.1968.9.23.66.

[7] T. Watanabe, M. Fujimaki, N. Fukunishi, H. Imao, O. Kamigaito, M. Kase, M. Komiyama, N. Sakamoto, K. Suda, M. Wakasugi, K. Yamada, Beam energy and longitudinal beam profile measurement system at the RIBF, in: Proc. 5th Int. Part. Accel. Conf. (IPAC 2014), 2014: pp. 3566–3568.

[8] J.F. Ziegler, J.P. Biersack, M.D. Ziegler, SRIM: the Stopping and Range of Ions in Matter, (2008).

http://www.srim.org.

[9] National Nuclear Data Center, Nuclear structure and decay data on-line library, Nudat 2.8, (2019). http://www.nndc.bnl.gov/nudat2/.

[10] International Atomic Energy Agency, LiveChart of Nuclides, (2009). https://www-nds.iaea.org/livechart/.

[11] B. Pritychenko, A. Sonzogni, Q-value Calculator (QCalc), (2003). http://www.nndc.bnl.gov/qcalc/.

[12] F. Tárkányi, S. Takács, K. Gul, A. Hermanne, M.G. Mustafa, M. Nortier, P. Obložinský, S.M. Qaim, B. Scholten, Y.N. Shubin, Z. Yousiang, Monitor Reactions 2007, updated version of charged particle cross-section database for medical radioisotope production, IAEA-TECDOC-1211, (2007). https://www-nds.iaea.org/medical/medical-old/monitor_reactions.html.

[13] A. Hermanne, A. V. Ignatyuk, R. Capote, B. V. Carlson, J.W. Engle, M.A. Kellett, T. Kibédi, G. Kim, F.G. Kondev, M. Hussain, O. Lebeda, A. Luca, Y. Nagai, H. Naik, A.L. Nichols, F.M. Nortier, S. V. Suryanarayana, S. Takács, F.T. Tárkányi, M. Verpelli, Reference Cross Sections for Charged-particle Monitor Reactions, Nucl. Data Sheets. 148 (2018) 338–382. https://doi.org/10.1016/j.nds.2018.02.009.

[14] A.J. Koning, D. Rochman, J. Sublet, N. Dzysiuk, M. Fleming, S. van der Marck, TENDL: Complete Nuclear Data Library for Innovative Nuclear Science and Technology, Nucl. Data Sheets. 155 (2019) 1–55. https://doi.org/10.1016/j.nds.2019.01.002.